Inorg. Chem. **2006**, *45*, 787–797

DFT-INDO/S Modeling of New High Molar Extinction Coefficient Charge-Transfer Sensitizers for Solar Cell Applications

Mohammad K. Nazeeruddin,*,† Qing Wang,† Le Cevey,† Viviane Aranyos,‡ Paul Liska,† Egbert Figgemeier,§ Cedric Klein,† Narukuni Hirata,|| Sara Koops,|| Saif A. Haque,|| James R. Durrant,|| Anders Hagfeldt,‡ A. B. P. Lever,*,⊥ and Michael Grätzel*,†

Laboratory for Photonics and Interfaces, Institute of Chemical Sciences and Engineering, School of Basic Sciences, Swiss Federal Institute of Technology, CH-1015 Lausanne, Switzerland, Department of Physical Chemistry, University of Uppsala, Box 532, SE-75121 Uppsala, Sweden, Department of Chemistry, University of Basel, Spitalstrasse 51, 4056 Basel, Switzerland, Centre for Electronic Materials and Devices, Department of Chemistry, Imperial College, Exhibition Road, SW7 2AZ London, U.K., and Department of Chemistry, York University, 4700 Keele Street, Toronto, M3J 1P3 Ontario, Canada

Received October 6, 2005

A new ruthenium(II) complex, tetrabutylammonium [ruthenium (4-carboxylic acid-4′-carboxylate-2,2′-bipyridine)-(4,4′-di(2-(3,6-dimethoxyphenyl)ethenyl)-2,2′-bipyridine)(NCS)$_2$] (N945H), was synthesized and characterized by analytical, spectroscopic, and electrochemical techniques. The absorption spectrum of the N945H sensitizer is dominated by metal-to-ligand charge-transfer (MLCT) transitions in the visible region, with the lowest allowed MLCT bands appearing at 25 380 and 18 180 cm^{-1}. The molar extinction coefficients of these bands are 34 500 and 18 900 M^{-1} cm^{-1}, respectively, and are significantly higher when compared to than those of the standard sensitizer *cis*-dithiocyanatobis(4,4′-dicarboxylic acid-2,2′-bipyridine)ruthenium(II). An INDO/S and density functional theory study of the electronic and optical properties of N945H and of N945 adsorbed on TiO_2 was performed. The calculations point out that the top three frontier-filled orbitals have essentially ruthenium 4d (t_{2g} in the octahedral group) character with sizable contribution coming from the NCS ligand orbitals. Most critically the calculations reveal that, in the TiO_2-bound N945 sensitizer, excitation directs charge into the carboxylbipyridine ligand bound to the TiO_2 surface. The photovoltaic data of the N945 sensitizer using an electrolyte containing 0.60 M butylmethylimidazolium iodide, 0.03 M I_2, 0.10 M guanidinium thiocyanate, and 0.50 M *tert*-butylpyridine in a mixture of acetonitrile and valeronitrile (volume ratio = 85:15) exhibited a short-circuit photocurrent density of 16.50 ± 0.2 mA cm^{-2}, an open-circuit voltage of 790 ± 30 mV, and a fill factor of 0.72 ± 0.03, corresponding to an overall conversion efficiency of 9.6% under standard AM (air mass) 1.5 sunlight, and demonstrated a stable performance under light and heat soaking at 80 °C.

1. Introduction

Energy consumption is expected to further rise steeply as a result of the increase in the world population and the rising demand of energy in developing countries. This is likely to enhance the depletion of fossil fuel reserves, leading to a further increase in greenhouse gas production and aggravation of the global warming problem.[1] The quality of life on earth is threatened unless renewable energy resources can be developed soon. This is one reason why the market for silicon solar cells is growing so rapidly. Nevertheless, the production of conventional silicon solar cells is expensive and also consumes high energy in fabrication. On the other hand, dye-sensitized solar cells (DSSCs) show promise and are potentially low in cost technology compared to the conventional silicon-based solar cells. These DSSCs consist

* To whom correspondence should be addressed. E-mail: MdKhaja.Nazeeruddin@epfl.ch (M.K.N.), blever@yorku.ca (A.B.P.L.), michael.graetzel@epfl.ch (M.G.).
† Swiss Federal Institute of Technology.
‡ University of Uppsala.
§ University of Basel.
|| Imperial College.
⊥ York University.

(1) Bilgen, S.; Kaygusuz, K.; Sari, A. *Energy Sources* **2004**, *26*, 1119.

10.1021/ic051727x CCC: $33.50
Published on Web 12/02/2005

of a sensitizer-immobilized mesoporous TiO_2 film deposited on a conducting transparent substrate (working electrode) and a platinum-sputtered conducting glass (counter electrode) sandwiched with an iodide/triiodide (I^-/I_3^-) redox electrolyte.[2] The immobilized sensitizer absorbs a photon to produce an excited state, which transfers efficiently its electron into the TiO_2 conduction band. The oxidized dye is subsequently reduced by electron donation from the iodide/triiodide redox system. The injected electron flows through the semiconductor network to arrive at the back contact and then through the external load to the counter electrode. At the counter electrode, reduction of triiodide, in turn, regenerates iodide, which completes the circuit. Such a simple system can reach solar to electric power conversion efficiencies of greater than 10%[3] and therefore have attracted the attention of several research groups.[4−26]

In these cells, the sensitizer is one of the key components for high-power conversion efficiency. The pioneering studies on dye-sensitized nanocrystalline TiO_2 films using *cis*-dithiocyanatobis(4,4′-dicarboxylic acid-2,2′-bipyridine)-ruthenium(II) (N3) are paradigms, which show metal/ligand-to-ligand charge-transfer (MLCT) transitions in the visible region at 25 000 and 18 700 cm^{-1} with a molar extinction coefficient of 14 000.[3] Despite this, the main drawback of this sensitizer is the lack of absorption in the red region of the visible spectrum and also the relatively low molar extinction coefficient. To increase further the efficiency of these cells, engineering of sensitizers at a molecular level is paramount.

The first requirement for the light-harvesting system of a molecular/semiconductor junction is that the sensitizing dye absorbs light over a wide wavelength range, encompassing as much of the visible spectrum as possible. Another essential property is that the sensitizer in the excited-state possesses directionality, providing an efficient electron transfer from the excited dye to the TiO_2 conduction band. Thus, good electronic coupling between the lowest unoccupied molecular orbital (LUMO) of the dye and the Ti 3d orbitals is required. In addition, the sensitizer should accomplish several demanding conditions: (i) its redox potential should be sufficiently high that it can be regenerated rapidly via electron donation from an electrolyte or a hole conductor, (ii) it should strongly exhibit absorbed visible radiation, so that dye solar cells could be made thinner and thus more efficient because of reduced transport losses in the nanoporous environment, (iii) it should possess a hydrophobic moiety on the ligand that increases the stability of the solar cells, and (iv) it should be stable enough to sustain many redox turnovers under illumination.

The above list of demanding desired properties for the sensitizer is well addressed by the synthesis of a ruthenium complex possessing different functionalized ligands. Toward this goal, we have designed and developed a new sensitizer, tetrabutylammonium [ruthenium (4,-carboxylic acid-4′-carboxylate-2,2′-bipyridine)(4,4′-di(2-(3,6-dimethoxyphenyl)-ethenyl)-2,2′-bipyridine)$(NCS)_2$] (hereafter labeled as N945H), constituted of different ligands with specific functionality. Note that the fully protonated version of this species is defined as N945H2 and the fully deprotonated version as N945. It is this fully deprotonated version that is actually attached to the TiO_2 films.

The purpose of incorporating carboxylic acid groups in the 4,4′ position of the 2,2-bipyridine ligand is twofold: to graft the dye on the semiconductor surface and to provide intimate electronic coupling between its excited-state wave function and the conduction band manifold of the semiconductor. The role of the thiocyanato ligands is to tune the metal t_{2g} orbitals of ruthenium(II) and possibly to stabilize the hole that is being generated on the metal, after having injected an electron into the conduction band. The function of the 4,4′-di(2-(3,6-dimethoxyphenyl)ethenyl)-2,2′-bipyridine ligand, which contains extended π conjugation with substituted methoxy groups, is to enhance the molar extinction coefficient of the sensitizer and, furthermore, to tune the LUMO level of the ligand to provide directionality in the excited state. In this paper, we report electronic,

(2) Grätzel, M. *Nature* **2001**, *414*, 338.
(3) Nazeeruddin, M. K.; Kay, A.; Rodicio, I.; Humphry-Baker, R.; Muller, E.; Liska, P.; Vlachopoulos, N.; Grätzel, M. *J. Am. Chem. Soc.* **1993**, *115*, 6382.
(4) Asbury, J. B.; Ellingson, R. J.; Gosh, H. N.; Ferrere, S.; Notzig, A. J.; Lian, T. *J. Phys. Chem. B* **1999**, *103*, 3110.
(5) Sugihara, H.; Sano, S.; Yamaguchi, T.; Yanagida, M.; Sato, T.; Abea, Y.; Nagaob, Y.; Arakawa, H. *J. Photochem. Photobiol. A: Chem.* **2004**, *166*, 81.
(6) Park, N.-G.; Kang, M. G.; Kim, K. M.; Ryu, K. S.; Chang, S. H.; Kim, D.-K.; Van de Lagemaat, J.; Benkstein, K. D.; Frank, A. J. *Langmuir* **2004**, *20*, 4246.
(7) Fabregat-Santiago, F.; Garcia-Canadas, J.; Palomares, E.; Clifford, J. N.; Haque, S. A.; Durrant, J. R.; Garcia-Belmonte, G.; Bisquert, J. *J. Appl. Phys.* **2004**, *96*, 6903.
(8) Heimer, T. A.; Heilweil, E. J.; Bignozzi, C. A.; Meyer, G. J. *J. Phys. Chem. A* **2000**, *104*, 4256.
(9) Lee, J.-J.; Coia, G. M.; Lewis, N. S. *J. Phys. Chem. B* **2004**, *108*, 5269.
(10) Ushiroda, S.; Ruzycki, N.; Lu, Y.; Spitler, M. T.; Parkinson, B. A. *J. Am. Ceram. Soc.* **2005**, *127*, 5158.
(11) Qiu, F. L.; Fisher, A. C.; Walker, A. B.; Petecr, L. M. *Electrochem. Commun.* **2003**, *5*, 711.
(12) Saito, Y.; Fukuri, N.; Senadeera, R.; Kitamura, T.; Wada, Y.; Yanagida, S. *Electrochem. Commun.* **2004**, *6*, 71.
(13) Adachi, M.; Murata, Y.; Takao, J.; Jiu, J.; Sakamoto, M.; Wang, F. *J. Am. Chem. Soc.* **2004**, *126*, 14943.
(14) Argazzi, R.; Larramona, G.; Contado, C.; Bignozzi, C. A. *J. Photochem. Photobiol., A: Chem.* **2004**, *164*, 15.
(15) Perera, V. P. S.; Senevirathna, M. K. I.; Pitigala, P. K. D. D. P.; Tennakone, K. *Sol. Energy Mater. Sol. Cells* **2005**, *86*, 443.
(16) Bisquert, J.; Cahen, D.; Hodes, G.; Ruehle, S.; Zaban, A. *J. Phys. Chem. B* **2004**, *108*, 8106.
(17) Cao, J.; Sun, J.-Z.; Hong, J.; Yang, X.-G.; Chen, H.-Z.; Wang, M. *Appl. Phys. Lett.* **2003**, *83*, 1896.
(18) Durr, M.; Bamedi, A.; Yasuda, A.; Nelles, G. *Appl. Phys. Lett.* **2004**, *84*, 3397.
(19) Furube, A.; Katoh, R.; Yoshihara, T.; Hara, K.; Murata, S.; Arakawa, H.; Tachiya, M. *J. Phys. Chem. B* **2004**, *108*, 12588.
(20) Hongwei, H.; Xingzhong, Z.; Jian, L. *J. Electrochem. Soc.* **2005**, *1*, 152.
(21) Kim, J. H.; Kang, M.-S.; Kim, Y. J.; Won, J.; Park, N.-G.; Kang, Y. S. *Chem. Commun.* **2004**, 1662.
(22) Kamat, P. V.; Haria, M.; Hotchandani, S. *J. Phys. Chem. B* **2004**, *108*, 5166.
(23) Nazeeruddin, M. K.; Humphry-Baker, R.; Officer, D. L.; Campbell, W. M.; Burrell, A. K.; Graetzel, M. *Langmuir* **2004**, *20*, 6514.
(24) Xue, B.; Wang, H.; Hu, Y.; Li, H.; Wang, Z.; Meng, Q.; Huang, X.; Sato, O.; Chen, L.; Fujishima, A. *Photochem. Photobiol. Sci.* **2004**, *3*, 918.
(25) Miyasaka, T.; Kijitori, Y. *J. Electrochem. Soc.* **2004**, *151*, A1767.
(26) Yamanaka, N.; Kawano, R.; Kubo, W.; Kitamura, T.; Wada, Y.; Watanabe, M.; Yanagida, S. *Chem. Commun.* **2005**, 740.

electrochemical, and photovoltaic properties of the N945 sensitizer.

2. Experimental Section

A. Materials. All of the solvents and chemicals, unless stated otherwise, were purchased from Fluka (purity grade). 4,4′-Dimethyl-2,2′-bipyridine (dmbpy), dichloro(*p*-cymene)ruthenium(II) dimer, and potassium/ammonium thiocyanate were obtained from Aldrich and used as received.

B. Measurements. UV/vis and fluorescence spectra were recorded in a 1-cm-path-length quartz cell on a Cary 5 spectrophotometer and a Spex Fluorolog 112 spectrofluorimeter, respectively. Electrochemical data were obtained by cyclic and square-wave voltammetry using a PC-controlled AutoLab PSTAT10 electrochemical workstation (Eco Chimie), where the Pt disk working electrode, Pt coil auxiliary electrode, and Ag disk quasi reference electrode were mounted in a single-compartment-cell configuration. The cyclic voltammogram of the N945H complex was obtained by dissolving 1 mM N945H complex in dimethylformamide (DMF) containing 0.1 M tetrabutylammonium hexafluorophosphate as the supporting electrolyte. After the measurement, ferrocene was added as the internal reference for calibration.[27]

^{1}H and ^{13}C NMR spectra were measured on a Bruker 200-MHz spectrometer. The reported chemical shifts were in ppm against tetramethylsilane. The Fourier transform infrared (FTIR) spectra were measured using a Digilab 7000 FTIR spectrometer. The attenuated total reflectance (ATR) data reported here were taken with the "Golden Gate" diamond-anvil ATR accessory (Graseby-Specac) typically using 64 scans at a resolution of 2 cm^{-1}. The IR optical bench was flushed with dry air. The FTIR spectra of anchored dyes were obtained by subtracting the IR spectrum of the blank TiO_2 films from the IR spectrum of the dye-coated TiO_2 films of the same thickness. Photoelectrochemical data were measured using a 450-W xenon light source that was focused to give 1000 W m^{-2}, the equivalent of one sun at air mass (AM) 1.5, at the surface of the test cell.

Electron injection dynamics were monitored using time-resolved single photon counting (TRSPC), employing an Edinburgh Instruments Fluorocube laser system. The apparatus employed 467-nm excitation (1-MHz repetition rate and an instrument response of 250-ps full width at half-height), with a 695-nm-high pass filter for emission detection. Transient absorption studies were conducted as reported previously,[28] both on dye-sensitized electrodes covered in propylene carbonate and on electrodes covered in the redox electrolyte [0.60 M 1-propyl-3-methylimidazolium iodide (PMII), 0.03 M I_2, 0.10 M guanidinium thiocyanate, and 0.50 M *tert*-butylpyridine in a mixture of acetonitrile and valeronitrile (volume ratio = 85:15)]. The samples were excited at 532 nm with low-excitation density pulses from a nitrogen-laser-pumped dye laser (<1-ns pulse duration, 0.8 Hz, intensity ~0.04 mJ cm^{-2}), and the resulting photoinduced change in the optical density was monitored at a probe wavelength of 800 nm.

The screen-printed double-layer film consists of a 10-μm transparent layer and a 4-μm scattering layer whose thickness was determined by using an Alpha-step 200 surface profilometer (Tencor Instruments, San Jose, CA). The electrodes were treated with a 0.05 M titanium tetrachloride solution using a previously reported procedure.[29] A porosity of 0.63 for the transparent layer was measured with a Gemini 2327 nitrogen adsorption apparatus (Micromeritics Instrument Corp., Norcross, GA). The film was heated to 500 °C in air and calcined for 20 min before use. Dye solutions were prepared in the concentration range of $(2-3) \times 10^{-4}$ M in a 1:1 (v/v) acetonitrile/*tert*-butyl alcohol solution, and the electrodes were dipped into the dye solution for 15−18 h. The dye-coated electrodes were rinsed quickly with acetonitrile and used as such for photovoltaic measurements. The fabrication procedure for solar cells, the testing conditions, and the equipment used were reported previously.[30]

Computational Methods. DFT calculations were carried out using the *Gaussian 03W* program suite.[31] Becke's three-parameter hybrid functional[32] with the LYP correlation functional[33] (B3LYP) was used together with the Los Alamos effective core potential LanL2DZ.[34] Molecular structures were initially obtained at the semiempirical INDO/1 level[35] to be used as starting input geometries. A tight self-consistent-field convergence criterion (10^{-8} hartree) was employed in all calculations. Harmonic frequency calculations were performed on all of the species at the level of theory of their optimization to establish the nature of the critical point (minimum or transition-point structure). The atomic orbital contributions to molecular orbitals and overlap populations were calculated using the AOMix program.[36]

The electronic spectra of the N945 suite of complexes were calculated with the INDO/S method in the Zerner implementation[37−41] using Hyperchem (version 7.5) software.[42,43] The singly excited configuration (CIS) approximation employed the DFT (B3LYP/LanL2DZ)-optimized geometries. The ruthenium and nitrogen atomic parameters of Krogh-Jespersen et al. were used.[44] The overlap weighting factors, f_σ and f_π, for INDO/S calculations were set at 1.267 and 0.585,[45,46] and the number of CISs in the CIS calculations was 1250 (25 occupied and 25 unoccupied orbitals).

The optical spectra of these ruthenium complexes were calculated using the SWizard program.[36,43] An absorption profile is calculated as a sum of Gaussian-shaped bands using the formula[34]

$$\epsilon(\omega) = 2.174 \times 10^9 \sum_I \frac{f_I}{\Delta_{1/2}} \exp\left[-2.773 \frac{(\omega - \omega_I)^2}{{\Delta_{1/2}}^2}\right] \qquad (1)$$

where molar absorbance ϵ is given in units of L mol^{-1} cm^{-1}. The

(27) Wolfbauer, G.; Bond, A. M.; Deacon, G. B.; MacFarlane, D. R.; Spiccia, L. *J. Am. Chem. Soc.* **2000**, *122*, 130.

(28) Hirata, N.; Lagref, J. J.; Palomares, E. J.; Durrant, J. R.; Nazeeruddin, M. K.; Graetzel, M.; Di Censo, D. *Chem.—Eur. J.* **2004**, *10*, 595.

(29) Nazeeruddin, M. K.; Péchy, P.; Renouard, T.; Zakeeruddin, S. M.; Humphry-Baker, R.; Comte, P.; Liska, P.; Le, C.; Costa, E.; Shklover, V.; Spiccia, L.; Deacon, G. B.; Bignozzi, C. A.; Gra1tzel, M. *J. Am. Chem. Soc.* **2001**, *123*, 1613.

(30) Nazeeruddin, M. K.; Humphry-Baker, R.; Liska, P.; Grätzel, M. *J. Phys. Chem. B* **2003**, *127*, 8981.

(31) Frisch, M. J.; et al. (see the Supporting Information for the full reference) *Gaussian 03W*, revision C.02; Gaussian, Inc.: Wallingford, CT, 2004.

(32) Becke, A. D. J. *Chem. Phys.* **1993**, *98*, 5648.

(33) Lee, C.; Yang, W.; Parr, R. G. *Phys. Rev.* **1988**, *B37*, 785.

(34) Hay, P. J.; Wadt, W. R. *J. Chem. Phys.* **1985**, *82*, 270.

(35) Dunning, T. H.; Hay, P. J. *Modern Theoretical Chemistry*; Plenum: New York, 1976.

(36) Gorelsky, S. I. AOMix program. http://www.sg-chem.net/aomix/.

(37) Ridley, J.; Zerner, M. C. *Theor. Chim. Acta* **1973**, *32*, 111.

(38) Ridley, J.; Zerner, M. C. *Theor. Chim. Acta* **1976**, *42*, 223.

(39) Zerner, M. C.; Loew, L. H.; Kirchner, R. F.; Mueller-Westerhoff, U. T. *J. Am. Chem. Soc.* **1980**, *102*, 589.

(40) Zerner, M. C.; Russo, N. *Metal−Ligand Interactions*; Kluwer Academic Publishers: Amsterdam, The Netherlands, 1996; p 493.

(41) Martin, C.; Zerner, M. C. In *Inorganic Electronic Structure and Spectroscopy*; Solomon, E. I., Lever, A. B. P., Eds.; Wiley: New York, 1999; Vol. 1, p 555.

(42) Gorelsky, S. I.; Lever, A. B. P. *J. Organomet. Chem.* **2001**, *635*, 187.

(43) Gorelsky, S. I. SWizard program. http://www.sg-chem.net/swizard/.

(44) Krogh-Jespersen, K.; Westbrook, J. D.; Potenza, J. A.; Schugar, H. J. *J. Am. Chem. Soc.* **1987**, *109*, 7025.

Scheme 1. Synthesis of 4,4′-(2-Hydroxy-2-(2,5-dimethoxyphenyl)ethenyl)-2,2′-bipyridine[a]

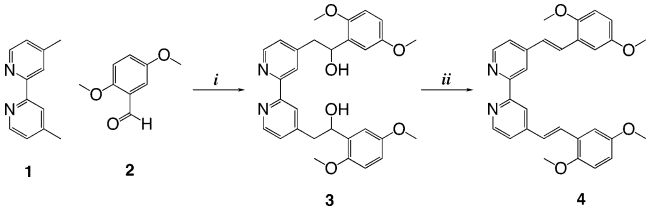

[a] Reagents and conditions: (i) THF, −40 °C, LDA and then **2**. (ii) CH_2Cl_2, TFAA, rt.

sum in eq 1 includes all allowed transitions with energies, ϵ_I (expressed in cm^{-1}), and oscillator strengths, f_I. The total integrated intensity under an absorption profile obtained from eq 1 is equal to a sum of the oscillator strengths:[1]

$$4.319 \times 10^{-9} \int \epsilon(\omega)\, d\omega = \sum_I f_I \qquad (2)$$

Half-bandwidths $\Delta_{1/2}$ were assumed to be equal to 3000 cm^{-1}, which is a typical half-bandwidth value for the complexes under consideration.

3. Synthesis and Characterization

A. Synthesis of 4,4′-Di(2,5-dimethoxyethenyl)-2,2′-bipyridine. Scheme 1 shows the synthetic strategy applied for the synthesis of the 4,4′-(2-hydroxy-2-(2,5-dimethoxyphenyl)ethyl)-2,2′-bipyridine. Lithium diisopropyl amide was formed under N_2 by mixing 3.72 mL of *n*-BuLi (1.6 M in hexane) with 0.78 mL of diisopropyl amine in 2 mL of tetrahydrofuran (THF) at −60 °C.[47] The mixture was stirred at room temperature for $^1/_2$ h. Then, a solution of 4,4′-dimethyl-2,2′-bipyridine (**1**; 0.5 g, 2.48×10^{-3} mol) in THF (1 mL) was added through a double-tipped needle at −40 °C. The black reaction mixture was then stirred at room temperature for 1 h. The aldehyde **2** (0.990 g, 5.96×10^{-3} mol) was dissolved in 1 mL of THF, and the resulting mixture was added to the reaction mixture as described above to form a yellow precipitate. After stirring for 1 h, the reaction was stirred into water and then extracted with dichloromethane. The organic phase was then washed with a saturated aqueous NaCl solution and dried over $MgSO_4$. The dried solution was concentrated and used in the next step without further purification.

The crude product **3** was dissolved in 15 mL of CH_2Cl_2 under nitrogen and added dropwise to trifluoroacetic anhydride (TFAA; 2 mL, 14.39×10^{-3} mol). During the addition, the reaction mixture turned orange. The mixture was stirred overnight and then concentrated to dryness. The resulting residue was dissolved in EtOAc (50 mL), washed with water (2×50 mL), dried over $MgSO_4$, and concentrated to dryness. The product was afforded as a yellow powder in 52.6% overall yield (0.627 g, 1.3×10^{-3} mol).

(45) Semiempirical Molecular Orbital Methods. In *Reviews in Computational Chemistry*; Zerner, M. C., Ed.; Wiley: New York, 1991; Vol. 2, pp 313−365.
(46) HyperChem for Windows, R. Professional Version; Hypercube Inc.: Gainesville, FL, 1997−2005.
(47) Aranyos, V.; Hjelm, J.; Hagfeldt, A.; Grennberg, H. *Dalton Trans.* **2003**, 1280.

^{1}H NMR ($CDCl_3$): δ 8.69 (2H, d, $J = 4.8$ Hz, pyridine), 8.61 (2H, s, pyridine), 7.47 (2H, $J = 16.4$ Hz, d, vinylic), 7.43 (2H, d, $J = 4.8$ Hz, pyridine), 7.32 (2H, t, $J = 7.6$ Hz, methoxyphenyl), 7.18 (2H, d, methoxyphenyl), 7.14 (4H, d, $J_1 = 16$ Hz, broad s, vinylic + methoxyphenyl), 6.90 (1H + 1H, d, $J_1 = 7.6$ Hz, broad s), 3.87 (s, 12H, $-OCH_3$). ^{13}C NMR: δ 49.5, 148.9, 133.3, 129.8, 126.4, 124.9, 122.2, 121.1, 119.7, 118.4, 114.5, 112.1, 55.3, 21.2. IR (KBr): 3306, 2937, 1598, 1487, 1462, 1435, 1263, 1149, 1046, 783, 700 cm^{-1}. Anal. Calcd for $C_{30}H_{28}N_2O_4$: C, 74.98; H, 5.87; N, 5.83. Found: C, 75.11; H, 5.81; N, 5.76.

B. Synthesis of Tetrabutylammonium [Ruthenium (4,-Carboxylic acid-4′-carboxylate-2,2′-bipyridine)(4,4′-di(2-(3,6-dimethoxyphenyl)ethenyl)-2,2′-bipyridine)-$(NCS)_2$] (N945H). A mixture of ligand 4,4′-di(2,5-dimethoxyethenylphenyl)-2,2′-bipyridine (0.192 g, 0.4 mM) and dichloro(*p*-cymene)ruthenium(II) dimer (0.12 g, 0.2 mM) in argon-degassed DMF (50 mL) was heated at 100 °C for 4 h (note: the temperature should not exceed 100 °C to avoid formation of the bis complex). Then, 4,4′-bis(carboxylic acid)-2,2′-bipyridine (0.098 g, 0.4 mM) was added, the temperature was raised to 160 °C, and the solution was refluxed for 4 h under reduced light (to avoid cis-to-trans isomerization). Subsequently, NH_4NCS (0.304 g, 4 mM) was added, and the solution was refluxed for a further 4 h at 140 °C. The DMF solvent was evaporated, and to the resulting purple residue was added water (15 mL); the mixture was then allowed stand in a refrigerator overnight at −4 °C. The resulting purple solid was filtered, successively washed with water, and dried. The dried product was further washed with diethyl ether.

The crude N945H complex was dissolved in methanol (5 mL) containing 2 equiv of tetrabutylammonium hydroxide to increase the solubility by deprotonating carboxylic acid protons. The concentrated solution was filtered through a sintered glass crucible (G4) and charged onto a Sephadex LH-20 column, which was prepared in methanol. The adsorbed complex was eluted using methanol. The main band was collected, and the solution pH was lowered to 5.1 using 0.02 M HNO_3 acid, which caused monoprotonation of the species, forming N945H. Then, the solution containing the precipitate was kept at −20 °C for 15 h. After the flask was allowed to warm to 25 °C, the precipitated complex was collected on a glass frit and air-dried. The same purification procedure was repeated five more times to obtain the pure N-bonded isomer complex.

Anal. Calcd for the mono(tetrabutylammonium salt) $C_{64}H_{87}N_7O_8RuS_2 \cdot H_2O$: C, 60.74; H, 7.09; N, 7.75. Found: C, 59.37; H, 7.30; N, 8.00.

^{1}H NMR (CD_3OD): δ_H 10.03 (d, $H^{6,5}$, $J = 5.9$ Hz), 9.97 (s, H^3), 9.90 (d, $H^{6',5'}$, $J = 5.8$ Hz), 9.81 (s, $H^{3'}$), 9.50 (s, $H^{3''}$), 9.35 (s, $H^{3'''}$), 8.93 (d, $H^{5,6}$, $J = 5.9$ Hz), 8.63 (d, $H^{5',6'}$, $J = 5.9$ Hz), 8.50 (d, vinyl H^7, $J = 15.87$ Hz), 8.35 (d, $H^{6'',5''}$, $J = 5.6$ Hz), 8.30 (d, vinyl $H^{7'}$, $J = 14.42$ Hz), 8.21 (d, $H^{6''',5'''}$, $J = 5.9$ Hz), 8.2 (m, $H^{5''}$, $H^{9,10,11}$), 8.19 (d, vinyl H^8, $J = 15.34$ Hz), 7.96 (d, vinyl $H^{8'}$, $J = 16.81$ Hz), 7.93 (d, $H^{5''',6'''}$, $J = 5.0$ Hz).

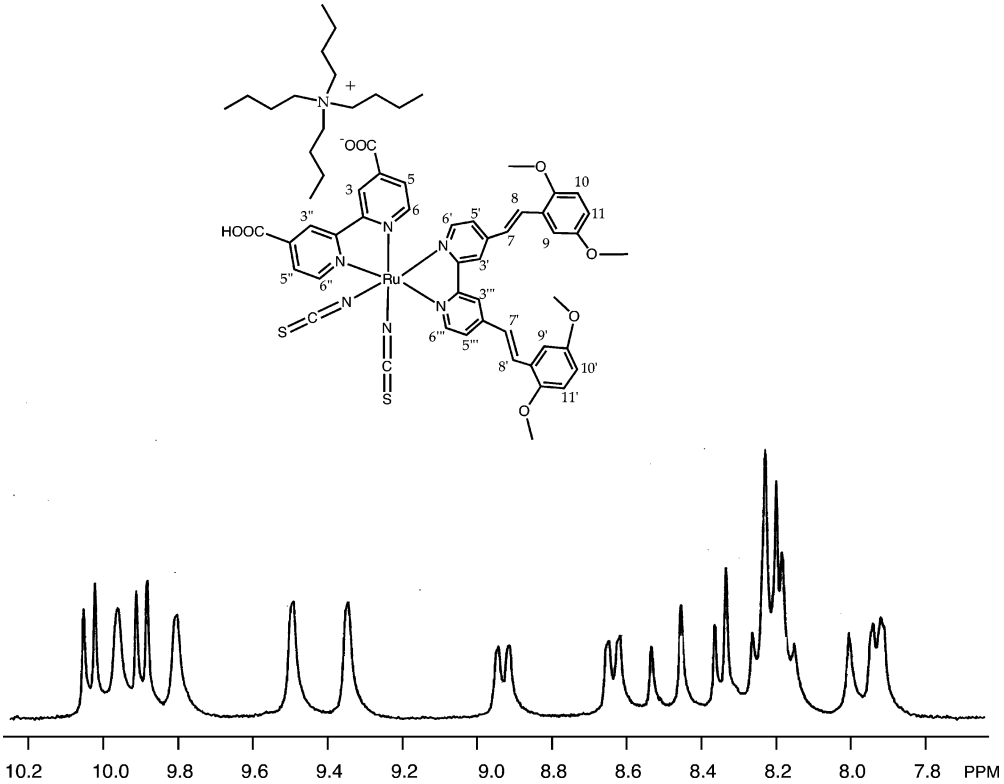

Figure 1. Chemical structure of the N945H complex and the numbering scheme showing our tentative assignments for NMR peaks (top panel). A portion of the ^{1}H NMR spectrum of the N945H complex measured in CD_3OD. For clarity, the peaks in the aliphatic region are not shown.

Aliphatic protons: 3.91 (s, $-OCH_3$), 3.85 (s, $-OCH_3$), 3.81 (s, $-OCH_3$), 3.74 (s, $-OCH_3$), 3.31 (m, $-CH_2$), 1.56 (m, $-CH_2$), 1.28 (m, $-CH_2$), 0.92 (t, $-CH_3$).

4. Results and Discussion

Synthesis. A two-step synthesis was used to afford the ligand 4,4′-di(2,5-dimethoxyethenylphenyl)-2,2′-bipyridine as shown in Scheme 1. First, a nucleophilic addition of the anion of **1** to *p*-2,5-methoxybenzaldehyde gave the corresponding alcohol **3**. Dehydration was achieved using TFAA followed by precipitation using acetic acid with an easy separation by chromatography for **4**. Figure 1 shows the structure of the ruthenium complex N945H, which was synthesized in a one-pot synthesis starting from a dichloro(*p*-cymene)-ruthenium(II) dimer in DMF for 12 h. The crude complex was purified on a Sephadex LH-20 column using methanol as an eluent. The complex was purified five times to remove S-bonded isomers. The analytical and spectroscopic data for N945H are fully consistent with the structure.

NMR Data. The ^{1}H NMR spectrum of the N945H complex is complicated because of the presence of two different ligands in which all of the pyridyl rings are electronically in a different environment. Therefore, the ^{1}H NMR spectrum shows the total number of resonances equal to the total number of aromatic protons in the complex. A portion of the ^{1}H NMR spectrum in the aromatic region is shown Figure 1b. The two doublets at δ 10.03 and 9.90 are assigned to the H^6 and $H^{6'}$ protons (see the structure in Figure 1a). The four singlet peaks at δ 9.97, 9.81, 9.50, and 9.35 are assigned to the H^3 protons of four pyridyl rings. The vinyl protons are clearly identified from the proton coupling constant data, which are 15−17 Hz, confirming that they are in a trans configuration. The resonance peaks in the aliphatic region are due to methoxy and tetrabutylammonium cation protons, and the integrated ratio of the aliphatic protons of tetrabutylammonium to aromatic protons shows the presence of one tetrabutylammonium cation per ruthenium center. The data confirm the absence of linkage isomers of the N945H complex due to N- and S-coordinated complexes, which were present in the crude complex to the extent of 10−15%.

The ^{13}C NMR spectrum of the N945H complex shows 40 resonance peaks in the aromatic region in which 12 carbon resonances are due to 4,4′-dicarboxylic acid-2,2′-bipyridine and 26 carbon resonances are due to 4,4′-di(2,5-dimethoxyethenylphenyl)-2,2′-bipyridine. No attempts were made to scrutinize individual aromatic carbons. However, the signals at δ 128.91 and 131.91 are assigned to the coordinated NCS ligand by comparison to the ^{13}C NMR spectrum of the N3 complex. In the aliphatic region, the peaks at δ 49.96, 24.77, 20.71, and 13.95 are due to tetrabutylammonium cation carbons. The peaks at δ 59.56, 59.51, 51.54, and 51.49 are assigned to methoxy carbons, which are downfield shifted, compared to the tetrabutylammonium carbons.

ATR-FTIR Spectra. The ATR-FTIR spectra of the N945H complex measured as a powder show a strong and intense absorption peak at 2098 cm^{-1} that is due to ν(CN), indicating that the NCS ligand is coordinated to the ruthenium center through an N atom. This band is approximately 1.8 times more intense than the band at 801 cm^{-1}, which is due to ν(CS). The bands at 1704 cm^{-1} (C═O) and 1220 cm^{-1} (C−O) are due to carboxylic acid

Table 1. Summary of Selected DFT-Optimized Bond Distances (pM)

	Ru−N-(bpyCO$_2$)	Ru−N-(bpy−ethenyl)	Ru−N-(NCS)	C═S
N945	208−209	204−206	207−208	169
N945H	205 (H),[a] 208	206−207	205−206	168
N945H2	204−205	208	205	167
N945[Ti(OH)$_3$]$_2$	204−206	207−208	205−206	167

[a] Refers to the ring carrying the CO_2H residue.

groups.[48] The bands at 1577 and 972 cm^{-1} are assigned to the characteristic C═C and trans C−H, respectively, of 4,4′-di(2,5-dimethoxyethenylphenyl)-2,2′-bipyridine. The 1577 cm^{-1} band is extensively overlapped with the asymmetric carboxylate band at 1605 cm^{-1} and appears as a distinct shoulder. The strong band at 1350 cm^{-1} is assigned to the symmetric band of the carboxylate group. The four bands at 1539, 1494, 1464, and 1423 cm^{-1} are due to the ring-stretching modes of the ligand. The bands at 2835, 2931, 2872, 2936, and 2959 cm^{-1} are due to ν(CH) of symmetric and asymmetric $-CH_2$ and $-CH_3$ groups, respectively.[48,49]

The ATR-FTIR data of the N945 complex after it has been anchored onto a 2-μm-thick nanocrystalline TiO_2 film reveal the mode of adsorption of this dye onto the TiO_2 surface. The ATR-FTIR spectra show clearly the absence of 1704 cm^{-1} (C═O) and the presence of the carboxylate asymmetric stretching vibration at 1604 cm^{-1} [$\nu(-COO^-_{as})$] and the symmetric vibration at 1381 cm^{-1} [$\nu(-COO^-_{s})$], confirming that the carboxylic acid proton is dissociated and involved in the adsorption on the TiO_2 surface; i.e., N945 is adsorbed (see Figure S1 in the Supporting Information).[30,48,50] It is worthwhile to point out that the 1600-cm^{-1} region is not exclusively in the carboxylate asymmetric mode but also involves bipyridyl ring modes. Therefore, the observed band at 1604 cm^{-1} could be due to both carboxylate and aromatic rings. The anchored N945 complex ν(CN) band of the NCS ligand and the characteristic ligand ring stretching modes are all moved to higher energy by 2−4 cm^{-1}. On the contrary, the ν(CS) mode of the NCS ligand slightly changed to lower energy 795 cm^{-1}. From these data, one infers that the dye is anchored on the surface through the carboxylate groups via a bridging of surface titanium ions rather than an ester-type linkage.[30]

Geometry Optimization. The geometries of N945, N945H, and N945H2 were optimized using DFT with a B3LYP/LanL2DZ functional and basis set. Selected bond distances are shown in Table 1. These fall well within the normal ranges for species of this type. There are trends, which are small but appear definite. Thus, the Ru−N bond to the carboxypyridine ligand is shorter than that to the ethenylpyridine ligand, and the former lengthens significantly with increasing negative charge (deprotonation) while the latter systematically decreases. The Ru−N(NCS) bond also lengthens with increasing negative charge on the carboxypyridine ligand, as does the C═S bond length. The ethenylpyridine ligand has a potential steric conflict between the "inner" methoxy groups. This steric interference could be minimized by twisting the ethenyl residues on the bypyridine ligand or by twisting the methoxy groups. DFT resolves this problem by keeping the entire ethenylpyridine ligand essentially coplanar (i.e., the methoxyethenyl residues lie in the same plane as the bipyridine rings) but by twisting the methoxy groups to minimize steric interference between them (Figure 2).

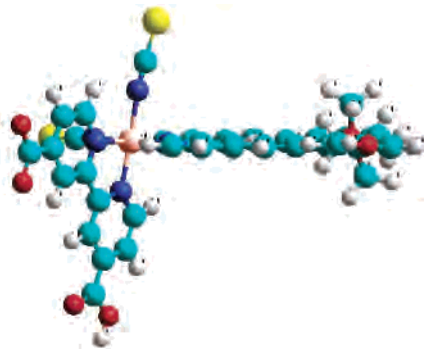

Figure 2. Optimized geometry of N945H. Color code: ruthenium, orange; carbon, light blue; hydrogen, white; oxygen, red; sulfur, yellow; nitrogen, dark blue. The orientation is shown to display the coplanarity of the ethenylbipyridine ligand.

We also geometry-optimized a titanium complex of N945, namely, N945[Ti(OH)$_3$]$_2$, where the [Ti(OH)$_3$]$^+$ groups are attached to a carboxyl oxygen atom on each carboxyl group of the N945 dianion; overall the species is neutral. This species was designed to mimic the possible binding of the N945 anion to the TiO_2 surface. Not too surprisingly, the bond distances in this species approximate to those of the neutral N945H2 species.

INDO/S Analysis and Electronic Spectra. Both INDO/S and time-dependent DFT (TD-DFRT) were used to predict the electronic spectra of these species. INDO/S gave better agreement with the experiment. Both predicted the lowest energy MLCT band at too low an energy relative to the experiment, and this is likely to be a consequence of the thiocyanate group carrying too negative a charge and hence decreasing the charge on the ruthenium center to a lower positive value than experimental reality. Both calculations are essentially gas phase, but the Zerner INDO parameters were obtained from solution-phase experimental data and are more appropriate than the DFT functional in circumstances where the solvent is likely to play an important role. In a solvent medium, the negative charge on the thiocyanate ion will be dispersed. This is mimicked better by the INDO/S calculation than by the TD-DFRT calculation. We therefore report the INDO/S analysis here. We have previously shown that both DFT and INDO give a fundamentally similar picture of the electronic behavior of ruthenium complexes.[42]

The frontier molecular orbital descriptions (INDO/S) of these complexes are displayed schematically in Figure 3a−d (tabulated data are given in the Supporting Information). We may suppose that electron injection from the excited sensitizer takes place from the lowest-energy spin-singlet or spin-triplet excited state depending on the relative rates of injection and intersystem crossing. In all of the species under

(48) Finnie, K. S.; Bartlett, J. R.; Woolfrey, J. L. *Langmuir* **1998**, *14*, 2744.
(49) Nazeeruddin, M. K.; Humphry-Baker, R.; Liska, P.; Graetzel, M. *J. Phys. Chem. B* **2003**, *107*, 8981.
(50) Shklover, V.; Ovehinnikov, Y. E.; Braginsky, L. S.; Zakeeruddin, S. M.; Grätzel, M. *Chem. Mater.* **1998**, *10*, 2533.

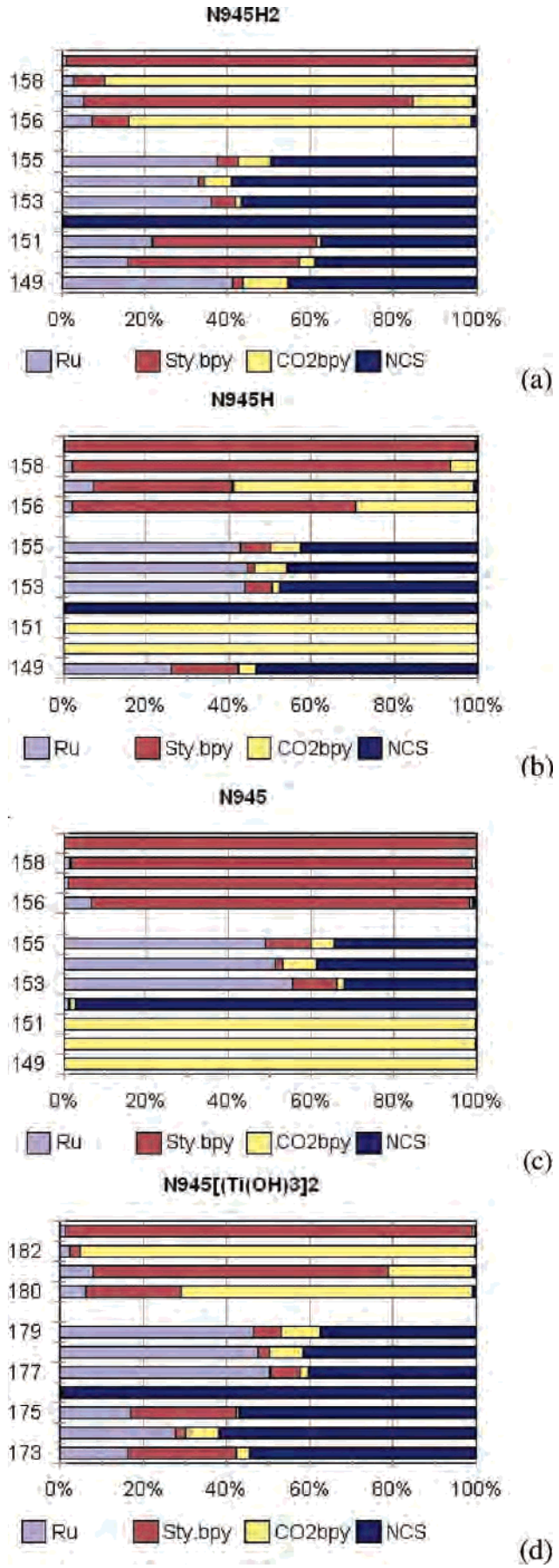

Figure 3. Percent composition of frontier orbitals in (a) N945, (b) N945H, (c) N945H2, and (d) N945[Ti(OH)$_3$]$_2$.

discussion, the lowest-energy spin-singlet state is a d → LUMO MLCT state while the lowest-energy spin-triplet state is an MLCT transition to the LUMO or LUMO+1 depending on the species. We are therefore interested primarily in the electron distribution in the LUMO and LUMO+1.

Consideration of Figure 3 a−d shows that the distribution over the carboxybipyridine and ethenylpyridine ligands is very dependent on the net charge on the carboxypyridine ligand. An additional negative charge has a dramatic effect in moving the π^* energy of the carboxypyridine ligand "up". Thus, for N945H2, the LUMO (and LUMO+2) is almost totally localized on the carboxypyridine ligand while the LUMO+1 is almost totally localized on the ethenylpyridine ligand, and there is little mixing between the π^* orbitals of carboxypyridine and ethenylpyridine. For the monoanion N945H, the LUMO is now mostly on ethenylpyridine but with a substantial contribution from carboxypyridine, while the reverse is true for the LUMO+1.

In the dianion N945, the π^* orbital of carboxypyridine has now moved substantially "up" and the LUMO and LUMO+1,2,3,4,5 are all almost exclusively localized on the ethenylpyridine ligand.

In the N945[Ti(OH)$_3$]$_2$ species, the carboxypyridine π^* orbital has again moved down, because of the positive field of the titanium(IV) atom, to become the principal contributor to the LUMO of the complex (Figure 3d). Assuming the LUMO is the critical molecular orbital crucial to electron injection into TiO_2, it is especially important that the titanium-bound model does direct electron transfer to the bipyridine bound to the titanium surface. Note that this would not be true if the surface species remains formally with two negative carboxyl functions; i.e., the orbitals would then be described as in N945 (Figure 3c).

The top three frontier-filled orbitals are 4d (t_{2g} orbitals in all cases but substantially mixed with thiocyanate π orbitals). This mixing is probably overemphasized because the thiocyanate charge is not dispersed.

Evidence for the reliability of this calculation can be obtained by comparing the calculated electronic spectrum (INDO/S) of these species with the experimental data. The absorption spectrum of the N945H sensitizer is dominated by two intense bands in the visible region at 25 380 and 18 180 cm^{-1}, assigned below as MLCT transitions. In addition, there are several bands in the UV region. The molar extinction coefficients of the lowest MLCT bands are 34 500 and 18 900 M^{-1} cm^{-1}, respectively, which are significantly higher than those of the standard sensitizer ″N3, whose visible-region MLCT band has an intensity of only 14 000 M^{-1} cm^{-1}. The lowest-energy MLCT band in the N945H complex is red-shifted 680 cm^{-1} and the molar extinction coefficient is increased by 35% when compared to the standard N3 sensitizer.

Figure 4 and Table 2 show, in addition to excellent agreement between observed and calculated spectra, a plethora of transitions in this low-symmetry species. Vertical bars show the predicted transitions, all of which below 30 000 cm^{-1} are MLCT in origin from Ru d to the lower-energy π^* orbitals of the bipyridine ligands. Details are shown in

Table 2. Electronic Absorption/Emission and Electrochemical Data of N945H

absorption:[a] λ_{max}, cm^{-1} (ϵ, 10^3 M^{-1} cm^{-1})	emission[b] λ_{max}, cm^{-1}	emission[b] τ, ns	E_{ox},[c] V	E_{ox},[c] V on TiO_2	E_{red},[c] V	E_{ox}*, V
32 680 sh (56.3), 31 640 (60.7), 25 380 (34.5), 18 180 (18.9)	12 120	27	0.81	1.01	−1.20, −1.61	−0.79

[a] Absorption data were obtained in a 1:1 acetonitrile/*tert*-butyl alcohol solution at 298 K. [b] Emission spectra were obtained by excitation at 18 180 cm^{-1}. [c] Electrochemical measurements were performed at 298 K using square-wave voltammetry on solutions in DMF containing 0.1 M $TBAPF_6$ as the supporting electrolyte. Potentials are quoted with respect to NHE.

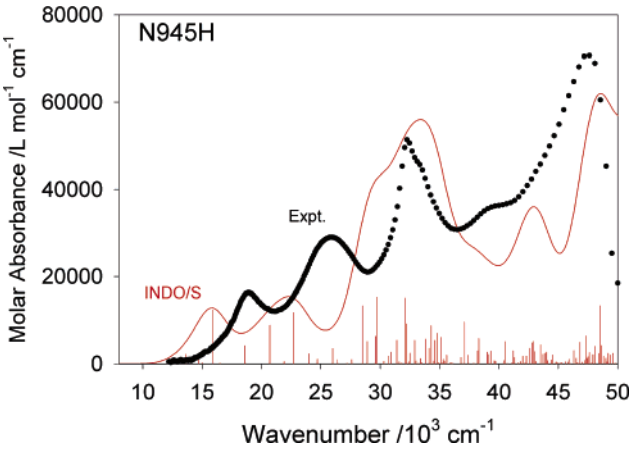

Figure 4. Experimental (recorded in methanol; black) and predicted (gas phase, INDO/S; red) spectra of N945H. The vertical red bars are the predicted oscillator strengths and locations of individual computed transitions. The oscillator strengths are arbitrarily magnified to match the overall spectrum; they retain their correct relative intensity.

Table 3. Predicted Spectrum[a] of N945H below 30 000 cm^{-1}

wavenumber, 10^3 cm^{-1}	oscillator strength	assignment[b]
13.6	0.055	155 → 156 (59%)
14.7	0.022	155 → 157 (29%), 154 → 156 (28%)
15.9	0.311	153 → 156 (38%), 154 → 157 (20%)
18.6	0.104	155 → 157 (40%)
20.7	0.223	155 → 158 (49%)
22.7	0.296	153 → 158 (41%)
24.0	0.058	155 → 160 (61%)
24.7	0.027	155 → 159 (55%)
26.0	0.090	154 → 160 (52%)
26.4	0.025	153 → 159 (38%)
27.6	0.025	151 → 156 (73%)
28.5	0.334	149 → 156 (24%)
28.9	0.130	149 → 156 (38%)
29.6	0.158	151 → 157 (33%)

[a] Only bands stronger than $f = 0.02$ are listed. [b] HOMO is 156 and LUMO is 157. The percentage is that of the dominant contribution. See Figure 3b to identify the composition of the orbitals.

Table 3. The low symmetry gives rise to quite complex spectra when analyzed in detail. The two apparent low-energy MLCT bands (below 30 000 cm^{-1}) contain at least eight spin-allowed MLCT transitions of nonzero intensity (Table 4). The asymmetry of the experimental data in this region provides definitive evidence for these many transitions. Each band is a composite of many transitions. The most one can say is that the two visible-region bands are primarily MLCT from Ru 4d to π^* of each bipyridine ligand while the higher-energy region (detailed assignments not shown) comprises higher-energy MLCT bands and interligand $\pi-\pi^*$ transitions.

When the N945H sensitizer is excited within the MLCT absorption band at 298 K in an air-equilibrated 1:1 aceto-

Table 4. Predicted Spectrum[a] of $N945[Ti(OH)_3]_2$ below 30 000 cm^{-1}

wavenumber, 10^3 cm^{-1}	oscillator strength	assignment[b]
12.8	0.03	179 → 180 (50%)
15.6	0.12	179 → 181 (38%), 179 → 180 (25%)
16.3	0.20	mixed assignment
18.6	0.12	177 → 181 (35%)
20.9	0.20	179 → 182 (53%)
22.0	0.23	179 → 183 (41%), 178 → 182 (39%)
23.1	0.33	177 → 183 (24%)
24.7	0.03	177 → 183 (49%)
24.9	0.06	178 → 183 (47%)
28.0	0.06	177 → 184 (49%)
28.4	0.29	176 → 181 (40%), 174 → 180 (25%)
28.6	0.03	174 → 180 (24%)
29.4	0.30	mixed assignment
29.5	0.17	175 → 180 (42%)

[a] Only bands stronger than $f = 0.02$ are listed. Oscillator strengths are rounded off to two decimal places because this is only a model system. [b] HOMO is 179, and LUMO is 180. The percentage is that of the dominant contribution. See Figure 3d to identify the composition of the orbitals.

nitrile/*tert*-butyl alcohol solution, it exhibits a luminescence maximum at 12 120 cm^{-1} (see Figure S3 in the Supporting Information) with an excited-state lifetime of 27 ns in a degassed solution. The lowest-lying triplet state from which emission presumably occurs is the HOMO → LUMO predicted at 9900 cm^{-1}. As above, this is predicted at too low an energy because of the negative charge of the thiocyanate groups not being adequately dissipated.

The absorption spectra of both N945 adsorbed on a 2-μm-thick TiO_2 film show features similar to those seen in the corresponding solution spectra but exhibit a slight red shift of 200 cm^{-1} as a result of the interaction of the anchoring groups to the surface (see Figure 5).[30]

The lowest-energy spin-singlet and spin-triplet state transitions both involve HOMO → LUMO excitation and are predicted (INDO/S) to lie at 12 800 and 9700 cm^{-1}, respectively. As noted above, the LUMO in the titanium-bound N945 is predominantly localized on the carboxypyridine ligand attached to the titanium surface (Figure 3a−d and Table 3). Molecular dynamics calculations have been used to model the interaction of the N719 complex with the (101) surface plane of anatase.[50] The most likely adsorption configuration of the N945 sensitizer on TiO_2 supported by IR analysis is that it is attached via two of carboxylate groups. The carboxylate either bridges two adjacent rows of titanium ions through bidentate coordination or replaces a surface hydroxyl group through a carboxylate anion.

Electrochemistry. (a) Ground-State Potentials. Figure 6 shows the cyclic voltammogram of the N945H complex obtained using a Pt disk electrode in a DMF solvent with 0.1 M tetrabutylammonium hexafluorophosphate. Upon scanning to positive potentials, the N945H complex exhibited

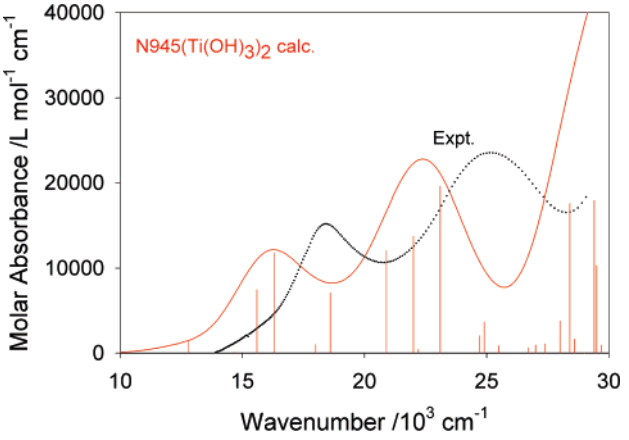

Figure 5. UV/vis absorption spectra of N945H complexes adsorbed as N945 on a nanocrystalline 2-μm-thick transparent TiO_2 film (black line). A similar 2-μm-thick TiO_2 nanocrystalline film was used as the reference. The INDO/S-calculated spectrum appears in red. The molar absorbance scale applies to the calculated spectrum. The absolute absorbance of the experimental data is not known; the data are arbitrarily scaled. The vertical red bars are the predicted oscillator strengths and locations of individual computed transitions. The oscillator strengths are arbitrarily magnified to match the overall spectrum; they retain their correct relative intensity.

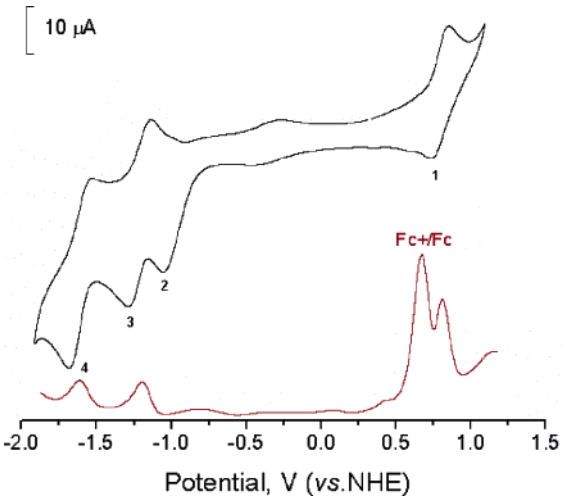

Figure 6. Cyclic voltammogram of the N945H complex measured in a DMF solution containing 0.1 M TBA(PF_6) using a Pt electrode with scan rate of 100 mV s^{-1}. The red curve shows the differential pulse voltammogram of the N945H complex with ferrocene as an internal reference. The direction of the measurement is from negative to positive potential, with a step potential of 10 mV, a modulation amplitude of 25 mV, modulation time of 0.05 s, and an interval time of 0.5 s.

a quasi-reversible metal-centered oxidation at $E_{1/2} = 0.81$ V vs NHE (labeled as 1 in Figure 6), with a separation of 0.09 V between the anodic and cathodic peaks, assigned to the $Ru^{III/II}$ couple (Figure 6). Under similar conditions, the N3 complex shows an oxidation process at 1.12 V vs NHE. When scanning is done toward negative potentials, one irreversible and two chemically reversible waves were observed. The irreversible wave (2) at $E_{1/2} = -1.05$ V is due to a reduction of the protons of the carboxylic acid of 4,4′-dicarboxylic acid-2,2′-bipyridine to hydrogen. Wolfbauer et al. have observed a similar behavior for the protons of the $dcbpyH_2$ ligand in the N3 complex at a platinum electrode.[27]

The two reversible waves (3 and 4) at $E_{1/2} = -1.20$ and -1.61 V vs NHE are assigned to the reduction of the species N945, not N945H, because once the proton has been reduced, the species at the surface of the electrode is the dianion N945. Reference to Figure 3c shows that the first four virtual π^* orbitals in N945 are localized on the ethenylpyridine ligand. Because the first four virtual π^* orbitals lie on the ethenyl ligand, it is possible that both reduction couples are localized on this ligand. However, once the first electron has been added, at equilibrium, the π^* orbitals on the ethenylpyridine ligand will rise in energy and possibly the next available empty orbital could then be π^* on the carboxy ligand. Therefore, the second reversible reduction couple is assigned to the carboxypyridine ligand, spectroelectrochemical studies are not carried out, and it would be necessary to prove this issue unambiguously.

(b) Excited-State Potentials. The excited-state oxidation potential of a sensitizer plays an important role in the electron-transfer process, for which an approximate value can be extracted from the ground-state oxidation couple and the zero−zero excitation energy $E^{(0-0)}$ according to eq 3.[51]

$$E(S^+/S^*) = E(S^+/S) - E^{(0-0)} \quad (3)$$

The $E^{(0-0)}$ energy (1.80 eV) was extracted from the high-energy side of the corrected emission spectra, where the intensity is 10% of the peak intensity (see Figure S3 in the Supporting Information). The oxidation potential of the excited state of the N945 sensitizer is −0.79 V vs NHE, which is notably more negative than that of the TiO_2 conduction band.[52] Therefore, this type of sensitizer could become very attractive, particularly for semiconductor materials having Fermi levels more negative than those of the TiO_2, where an increased gap between the conduction band and the redox couple will result in a higher open-circuit potential that increases the cell efficiency considerably. On the other hand, the oxidation potential of the N945 sensitizer is more positive than the I^-/I_3^- redox couple. The gain in the excited-state oxidation potential was obtained without appreciably sacrificing the ground-state oxidation potential, which is vital for regeneration of the dye by the redox couple.

Injection Dynamics. TRSPC was employed to monitor the electron injection kinetics from the N945 excited state into the TiO_2 conduction band. Typical data are shown in Figure 7, including control data employing a N945-sensitized nanocrystalline ZrO_2 film and data for N945-sensitized TiO_2 films covered in both an inert solvent and a redox couple. ZrO_2 was employed for the control data because its high conduction band edge prevents electron injection from the dye in the excited state. For this control film, a biphasic decay is observed, with lifetimes (amplitudes) of 3 ns (0.2) and 31 ns (0.8). For the TiO_2 films covered in an inert solvent, this emission is strongly quenched, consistent with efficient electron injection from the N945 excited state. Compared to the data for the TiO_2 films covered in an inert solvent, the decay dynamics are significantly slower in the presence

(51) Kuciauskas, D.; Monat, J. E.; Villahermosa, R.; Gray, H. B.; Lewis, N. S.; McCusker, J. K. *J. Phys. Chem. B* **2002**, *106*, 9347.
(52) Liu, G.; Jaegermann, W.; He, J.; Sundströlm, V.; Sun, L. *J. Phys. Chem. B* **2002**, *106*, 5814.

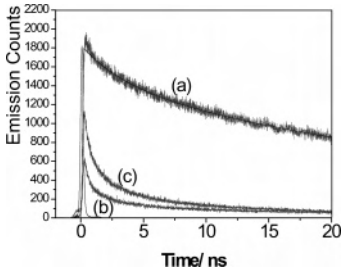

Figure 7. Time-resolved emission decays for N945-sensitized nanocrystalline films. Data (dark gray lines) are shown for (a) N945 on ZrO_2 covered in propylene carbonate/ethylene carbonate (PC/EC), (b) N945H on TiO_2 covered in PC/EC, and (c) N945 on TiO_2 covered in the redox electrolyte (0.6 M tetrabutylammonium iodide, 0.1 M lithium iodide, 0.5 M 4-*tert*-butylpyridine, and 100 mM iodine dissolved in propionitrile). Also shown (black lines) are the instrument response and the biexponential fit to the ZrO_2 data. Data collected for matched sample optical densities and data collection times, allowing direct comparison of the magnitudes of the emissions signals.

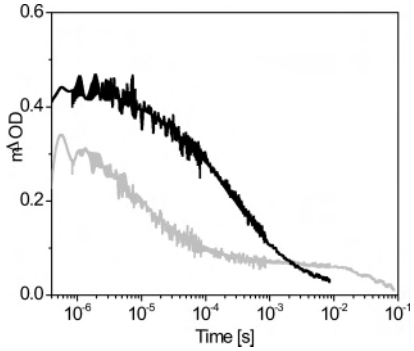

Figure 8. Transient absorption data for N945H-sensitized TiO_2 films covered in propylene carbonate (black trace) and a redox electrolyte (gray trace). Data were collected at a probe wavelength of 800 nm, following pulsed excitation at 532 nm.

of a redox electrolyte, with a half-time on the order of 100 ps. These slower decay dynamics observed in the presence of electrolyte are assigned, as we have discussed previously,[53] to the influence of the redox electrolyte on the TiO_2 conduction band energetics, thereby resulting in slower electron injection dynamics. Previous studies have shown that the TiO_2 conduction band energetics are strongly dependent upon the electrolyte composition.[54] A comparison with data collected for N3-sensitized films collected under the same experimental conditions indicates that electron injection dynamics for the N945 dye are approximately twice as fast as those observed for N3. These fast electron injection dynamics are consistent with those of the dye excited state being localized on the carboxypyridine groups closest to the TiO_2 substrate, as indicated by the DFT-INDO/S calculations.

Transient absorption studies (Figure 8) were employed to monitor the charge recombination and dye re-reduction of N945 adsorbed to nanocrystalline TiO_2 films covered in an inert solvent (black trace) and an iodine/iodide redox electrolyte (gray trace). In an inert solvent, the transient signal (monitored at 800 nm) is assigned primarily to photoinduced absorption of the N945 cation formed by electron injection

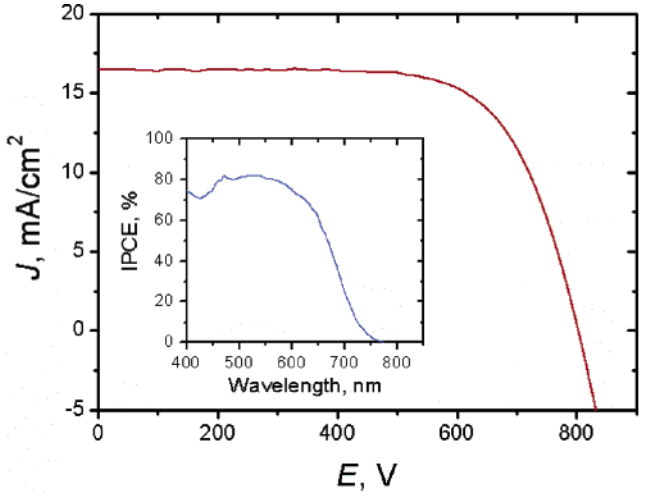

Figure 9. Photocurrent−voltage curve of a solar cell based on the N945 sensitizer measured under AM 1.5 sunlight illumination (100 mW cm^{-2}) (red line). The cell is masked with black plastic to avoid diffusive light, leaving an active cell area of 0.158 cm^2. The inset shows a photocurrent action spectrum obtained with the N945 complex attached to a nanocrystalline TiO_2 film. The IPCE is plotted as a function of wavelength of the excitation light.

into the TiO_2 electrode.[55] The decay of this photoinduced absorption is assigned to charge recombination of these N945 cations with photoinjected electrons. The half-time for this decay is 150 μs, indicative of the long-lived charge-separated state necessary for efficient photovoltaic device function. In the presence of a redox electrolyte, a rapid (half-time of ~2 μs) decay of this photoinduced absorption is observed, assigned as previously to regeneration of the dye ground state by electron transfer from iodide ions in the electrolyte.[56] Following this rapid decay, a long-lived signal is observed (half-time of 0.4 s) assigned to long-lived I_2^- species generated by the regeneration reaction and associated with TiO_2 electron absorption.[56] When these kinetics are compared with control data observed for the N3 dye, the recombination dynamics to the N945 dye cation are approximately 1 order of magnitude faster while the regeneration dynamics for N945 are slightly slower than those for N3. Nevertheless, the regeneration dynamics remain fast relative to the charge recombination to the dye cation, resulting in the overall charge-separation efficiency of electron injection and iodide oxidation [as determined by the yield of the $TiO_2(e^-)/I_2^-$ species monitored by the long-lived 800-nm signal] being indistinguishable between the two dyes and confirming the potential of this dye to achieve efficient photovoltaic device function.

Photovoltaic Data. The inset in Figure 9 shows the photocurrent action spectra of N945-sensitized solar cells based on a double-layered nanocrystalline TiO_2 film with an electrolyte consisting of 0.60 M PMII, 0.03 M I_2, 0.10 M guanidinium thiocyanate, and 0.50 M *tert*-butylpyridine in a mixture of acetonitrile and valeronitrile (volume ratio = 85:15). The incident monochromatic photon-to-current con-

(53) Haque, S. A.; Palomares, E.; Cho, B. M.; Green, A. N. M.; Hirata, N.; Klug, D. R.; Durrant, J. R. *J. Am. Chem. Soc.* **2005**, *127*, 3456.
(54) Haque, S. A.; Tachibana, T.; Willis, R. L.; Moser, J. E.; Gratzel, M.; Klug, D. R.; Durrant, J. R. *J. Phys. Chem. B* **2000**, *104*, 538.
(55) Klein, C.; Nazeeruddin, M. K.; Liska, P.; Censo, D. D.; Hirata, N.; Palomares, E.; Durrant, J. R.; Grätzel, M. *Inorg. Chem* **2005**, *44*, 178.
(56) Montanari, I.; Nelson, J.; Durrant, J. R. *J. Phys. Chem.* **2002**, *106*, 12203.

version efficiency plotted as a function of the excitation wavelength shows a plateau region with yields above 82%. From the overlap integral of this curve, one measures a short-circuit photocurrent density of 16.1 mA cm^{-2}. In agreement with this measurement, the N945-sensitized cell gave, under standard global AM 1.5 solar conditions, a short-circuit photocurrent density (i_{sc}) of 16.50 ± 0.20 mA cm^{-2}, an open-circuit voltage (V_{oc}) of 790 ± 30 mV, and a fill factor (ff) of 0.72 ± 0.03, corresponding to an overall conversion efficiency η, derived from the equation $\eta = i_{sc}V_{oc}$ff, of 9.64%.

DSSCs with electrolyte-containing, low-boiling-point solvents are not practicable for long-term applications. Therefore, we have developed a thermally stable electrolyte composed of 0.8 M 1,2-dimethyl-3-propylimidazolium iodide, 0.1 M I_2, and 0.5 M *N*-methylbenzimidazole in 3-methoxypropionitrile, which is a low-vapor-pressure, high-boiling solvent. Using this electrolyte system, the photovoltaic performance of the N945 sensitizer was investigated. Strikingly, the sensitizer exhibited a short-circuit photocurrent density of 16 ± 0.5 mA cm^{-2}, an open-circuit potential of 752 ± 20 mV, and a fill factor of 0.69 ± 0.05, yielding a power conversion efficiency of 8.4% under AM 1.5 full sunlight. However, at a light intensity of half a sun, the short-circuit photocurrent density was 8 ± 0.5 mA cm^{-2}, the open-circuit potential 752 ± 20 mV, and the fill factor 0.74 ± 0.05, yielding a power conversion efficiency of 9.0%. The increased efficiency at half a sun is mainly due to the improved fill factor. Under similar conditions, the K19 sensitizer gave a short-circuit photocurrent density of 14.61 mA cm^{-2}, an open-circuit photovoltage of 711 mV, and a fill factor of 0.67, yielding an overall conversion efficiency (η) of 7.0%.[57]

The excellent efficiency of the N945 DSSC compared to that of the N719 sensitizer is mainly due to a strong optical light absorbance across the visible spectrum and a superior response in the red region.[58] From the electronic and photovoltaic data, it is apparent that the significant effect asserted by the N945 sensitizer that contains a ligand with an extended π conjugation with donor groups in the ortho and meta positions is a higher efficiency compared to the N719 sensitizer.

The N945 DSSCs were subjected to accelerated testing in a solar simulator at 100 mW cm^{-2} intensity and in an oven at 80 °C. The cells showed excellent photochemical and thermal stability, and the efficiency remained 95% of the initial value after 35 days of thermal stress at 80 °C. The full details of the stability data are beyond the scope of this paper and are subject to a forthcoming paper.[59]

4. Conclusions

In summary, we have demonstrated selective functionalization of a ruthenium complex, resulting in red-shifted absorption spectra and enhanced molar extinction coefficient of the sensitizer. Our finding allows the creation of directionality in the excited state of the sensitizer by adjusting the electron densities of the donor moieties that are not attached to the TiO_2 surface, which is a key step for the future design and development of new molecules for solar cell applications. We are examining other related complexes that contain substituents in both the ortho, meta, and para positions of the π-extended ligand, which offer the possibility of shifting the LLCT/MLCT absorption maxima significantly to the red.

Acknowledgment. We acknowledge financial support of this work by the Swiss Science Foundation, Swiss Federal Office for Energy (OFEN), and U.S. Air Force Research Office under Contract No. F61775-00-C0003. A.B.P.L. thanks the Natural Sciences and Engineering Research Council (NSERC), Ottawa, Canada, for financial support. J.R.D. acknowledges financial support of the EPSRC (Supergen) program. We thank Dr. Robin Humphry-Baker, Dr. S. M. Zakeeruddin, Dr. Peter Péchy, and Pascal Comte for their kind assistance.

Supporting Information Available: ATR-FTIR data, emission spectra, and the INDO/S calculations showing calculated transitions and intensities of these sensitizers. This material is available free of charge via the Internet at http://pubs.acs.org.

IC051727X

(57) Wang, P.; Klein, C.; Humphry-Baker, R.; Zakeeruddin, S. M.; Grätzel, M. *J. Am. Ceram. Soc.* **2005**, *127*, 808.
(58) Zukalova, M.; Zukal, A.; Kavan, L.; Nazeeruddin, M. K.; Liska, P.; Graltzel, M. *Nanoletters* **2005**, *5*, 1789.
(59) Cevey, L.; Nazeeruddin, M. K.; Grätzel, M. *Sol. Energy Mater.* **2005**, in preparation.